PROCEEDINGS OF SPIE

SPIEDigitalLibrary.org/conference-proceedings-of-spie

Experimental results of an innovative dynamic low-coherent interferometer for characterizing a gravitational wave detector

Jesús Vilaboa Pérez, Marc Georges, Juriy Hastanin, Jérôme Loicq

Jesús Vilaboa Pérez, Marc Georges, Juriy Hastanin, Jérôme Loicq, "Experimental results of an innovative dynamic low-coherent interferometer for characterizing a gravitational wave detector," Proc. SPIE 12672, Applied Optical Metrology V, 126720F (4 October 2023); doi: 10.1117/12.2677489

SPIE.

Event: SPIE Optical Engineering + Applications, 2023, San Diego, California, United States

Experimental results of an innovative dynamic low-coherent interferometer for characterizing a gravitational wave detector

Jesús Vilaboa Pérez[a,*], Marc Georges[a], Juriy Hastanin[a], and Jérôme Loicq[a,b]

[a]Centre Spatial de Liège (CSL), STAR Institute, Université de Liège, Avenue du Pré-Aily, 4031, Liège, Belgium

[b]Faculty of Aerospace Engineering, Delft University of Technology, Delft, 2629 HS, Netherlands

ABSTRACT

We present the experimental results of the proof of concept of a metrology instrument developed to characterize the cryogenic mirror of the Einstein Telescope (ET) prototype. ET is a proposed gravitational-wave observatory. The metrology instrument uses the principle of low-coherence interferometry to measure the local change in topology and local induced vibrations of the mirror resulting from the cooling down process. We implement an innovative optical phase mask and a microlens array to obtain a depth map of the mirror on a single camera frame. With our instrument prototype, we can obtain 25 interference patterns of the same mirror spot for each camera frame. Each interference pattern corresponds to a difference Optical Path Difference (OPD). Then by reconstructing the interference patterns, we can measure the mirror's local topology change and local induced vibration. Moreover, in this proceeding, we describe the analysis of the white-light interference patterns through numerical simulations and depict the metrology instrument's optical design. Finally, we discuss how we can use the metrology instrument for real-time characterization of other optical components with all the advantages of white light interferometry.

Keywords: White Light Interferometry, Dynamical Interferometry, Optical Phase Mask, Single-Frame low-coherence Interferometry, Gravitational Wave Detector

1. INTRODUCTION

Low-coherence interferometry, or white light interferometry, is a commonly used metrology technique to characterize optical components. Some of the advantages of white light interferometry are: we can avoid the 2 π ambiguity of conventional high-coherence sources, we can determine with unambiguity the position of the mirror, and we can reduce the number of spurious unwanted interferometry signals[1,2,3] Most commonly, we use low-coherence interferometry for surface topology characterizations while we can also apply it for other applications such as the measurement of out-plane induced vibrations.[4]

The white light interferogram is characterized by a well-differentiated central fringe visible only within the limits of the coherence length of the source. The peak of the coherence envelope that wraps the central fringe of the interferogram gives us the data on the topology or position of the mirror. There are several techniques to find this coherence peak with nanometer precision. Some of these techniques look directly to the highest point of the envelope, as the well-known centroid method. In contrast, other techniques depict a more sensitive approach that makes use of the white light interference phase as the Phase Shifting Interferometry (PSI) method[5,6,7]

In this paper, we present the conceptual design, numerical simulations and the first experimental results of an innovative low-coherence interferometer that simultaneously measures local topology changes and local induced vibrations. The metrology instrument contains an optical phase mask for performing dynamic or real-time interferometry. The optical phase mask has a step design where each step introduces a different OPD to the rays that go through and come from the same mirror spot. The objective is to acquire a set of interference patterns of the same spot on the mirror with a single camera frame, each at a different OPD. Then, with the interference patterns, we can reconstruct the white light interferograms and, consequently, determine the local topology of the mirror. We use two consecutive camera frames to determine the local induce vibration as the displacement of the peak of the coherence envelopes between two camera frames. In our work, we address the frequency range of induced vibration from 0.1 Hz to 10 Hz and precision on the topology measurements of a few

Applied Optical Metrology V, edited by Erik Novak, Christopher C. Wilcox, Proc. of SPIE
Vol. 12672, 126720F · © 2023 SPIE · 0277-786X · doi: 10.1117/12.2677489

nanometers. In this paper, we present the results obtained with a proof of concept of the metrology instrument containing a custom optical phase mask of 5 by 5 steps. We analyze the results and discuss a second iteration of the instrument.

The research we carried out is under the frame of the E-TEST prototype for the Einstein Telescope. E-TEST includes a cryogenic mirror or gravitational wave detector suspended by an innovative hanging module[8,9].[10] Due to the extreme temperature changes, the topology of the cryogenic mirror may change. Moreover, the mirror may vibrate at low frequencies even with the active hanging module. Accordingly, the characterization of these two effects is essential to ensure the accuracy of the results in detecting gravitational waves.

It is important to note that the developed instrument is also helpful in inspecting other optical components. Thanks to the dynamic aspects inherent in the proposed approach, we can use it for fast characterizations with the resolution of low-coherence interferometry.

2. METHODS

2.1 Measurement principle

With our metrology instrument, we can obtain all the data points needed to reconstruct the local interferogram on a single camera frame. Then, by numerically analyzing the interferograms, we can derive the value of the local topology change and the local induced vibration of the mirror. To perform dynamic interferometry, we designed an innovative optical phase mask consisting of a grid of steps of different optical thicknesses, in which each step introduces a different OPD to the rays reflected from the same local point on the mirror. Accordingly, the optical phase mask replaces a traditional motorized stage used to do a depth scan of the mirror surface.

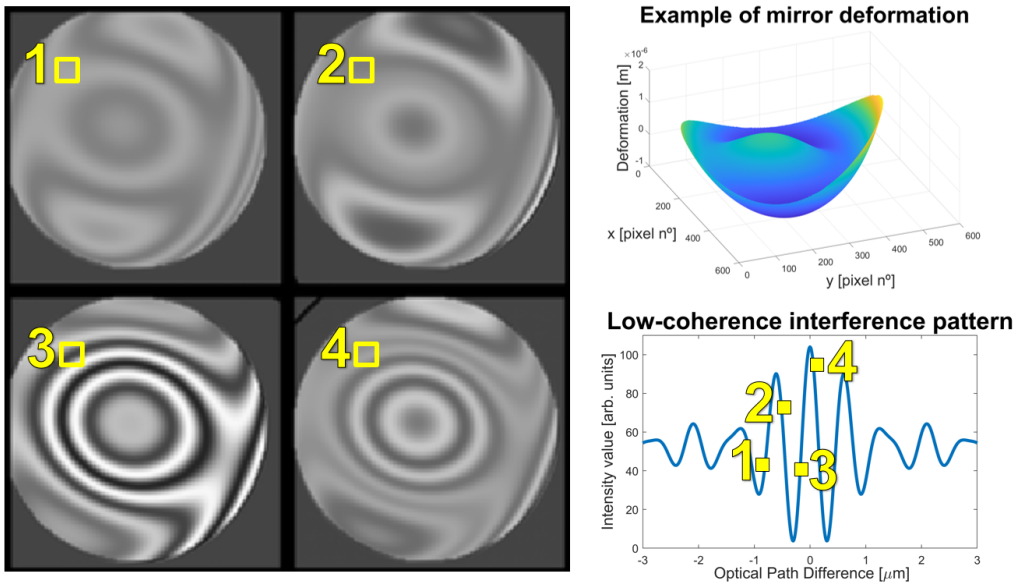

Figure 1. Illustration of the first application of the metrology instrument we developed, the measurement of local changes on the topology of the mirror. a) Ray tracing software ASAP NextGen optical simulation of the interference patterns obtained with an optical phase mask of four steps of the example of mirror deformation (b). c) Reconstruction of the white light interferogram for one point. For the simulations, we used a white light source of 200 nm bandwidth in the visible from 400 nm to 600 nm with a central wavelength at 550 nm

Figure 1 depicts the computer simulation for the first application of the instrument, the measurement of local changes in the topology of the mirror. We used an optical phase mask of 2 by 2 steps and a light source of 200 nm bandwidth in the visible from 400 nm to 600 nm with a central wavelength at 550 nm. Figure 1 a) represents the four interference patterns of the example of mirror deformation of Fig. 1 b) that we measure at

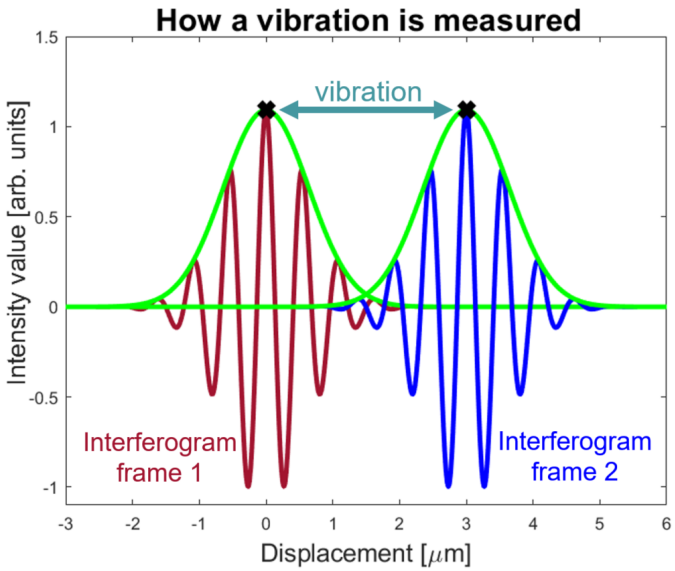

Figure 2. Illustration of the second application of the metrology instrument we developed, detecting local induced vibrations. We measure a local induced vibration as the displacement of the peak of the coherence envelope of the local interferogram at two consecutive camera frames. The temporal resolution of the measurements depends on the frame rate of the camera used

the detector. Each interference pattern corresponds to the same mirror spot, representing each a different OPD. In Fig. 1 c), we illustrate the reconstruction of the white light interferogram for one of the local points inside the mirror spot under characterization. Then, by determining the peak of the coherence envelope of the white light interferogram, we can get the local topology value of the mirror for that camera frame. It is important to note that the mirror topology may change between camera frames due to the extreme temperature variations of the cryogenic mirror under test. To determine the peak of the coherence envelope, we need an analysis method compatible with the optical phase mask we developed. On one side, we are limited by the number of sample points, one sample point for each step of the optical phase mask, since the technology to manufacture such a mask is under development. Conversely, we found limitations in traditional analysis methods such as the PSI method. The PSI method requires a set of sample points equidistant in terms of phase shift. In our case, since we use a polychromatic source and an optical phase mask of a single material, which introduces a different phase shift depending on the wavelength, we could not ensure equidistant values in terms of phase shift; therefore, we could not achieve our desired resolution. One of the solutions we propose is to determine the peak of the coherence envelope by a Hilbert transform or by a function like the product of a cosine and a Gaussian function to fit the intensity points. The analysis of the interferograms will be the object of a future publication.

The second application is the measurement of local induced vibrations of the E-TEST mirror, which is suspended and at cryogenic temperatures. For this application, we use the pair of local interferograms obtained in two consecutive camera frames. First, using an analysis method for the white light interferograms, we locate the peak of the coherence envelope of each interferogram. We then use the distance between the identified peaks to compute the local vibration between two frames. This distance should be zero in a perfect scenario where the mirror is completely isolated from vibrations. We illustrate the procedure in Fig. 2. In this figure, we normalize the intensity to a value between -1 to 1, but the intensity values are always positive. Then, we can repeat the procedure with all the local points of the mirror spot we characterize. We target the range of induced vibrations between 0.1 Hz to 10 Hz. The height difference between the smaller and larger step of the optical phase mask gives the maximum range of motion. The measurement's precision is directly related to the precision determining the peak of the coherence envelope.

2.2 Optical layout

Figure 3 illustrates the schematic optical layout of the metrology instrument we developed. We made use of the basis of a Michelson Interferometer, and we implemented the following components: a lens (7) and (4) before the reference (8) and measurement (5) mirrors; an optical phase mask on the reference arm (6); a diffuser (2) before the cube beam splitter (CBS) (3); and a microlenses array (9) before the detector (10). We start by spatially filtering and collimating the light (1). Then we redirect the light through the diffuser, which simulates an extensive array of point sources and creates a uniform optical field. Next, we use a CBS to split and recombine the light beam and to avoid using a compensation plate which would have complicated the alignment process. Finally, we implemented a microlenses array before the detector to focus the light rays. The number of microlenses of the microlenses array is equivalent to the number of steps of the optical phase mask. The lenses of the array are square-shaped with identical dimensions to the steps of the phase mask. Accordingly, we have an interferogram pattern for each pair of optical phase mask step and microlense.

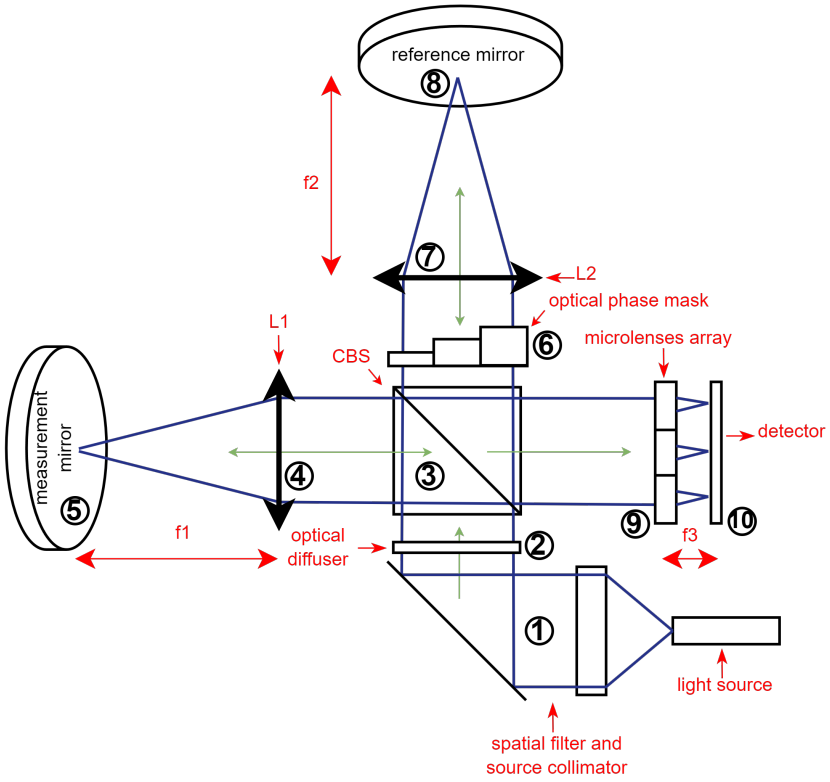

Figure 3. Optical layout of the metrology instrument to characterize local changes in the topology of a mirror and local induced vibrations. Each pair of microlense (6) and step of the optical phase mask (9) is related to the measurement of a different interference pattern of the same mirror spot at the detector.

We implemented the instrument's optical layout on a proof of concept at the laboratory. The proof of concept includes a custom-made optical phase mask of 5 by 5 steps and a microlenses array of also 25 microlenses. The detector is an Allied Vision Prosilica GE-2040 1.2" Monochrome CCD Camera modified with 3D printed components. We depict the proof of concept in Fig. 4.

3. RESULTS

Figure 4 depicted the proof of concept we developed at the laboratory to confirm the numerical results for the measurement principle of the instrument. For this first iteration of the metrology instrument, we used a source of

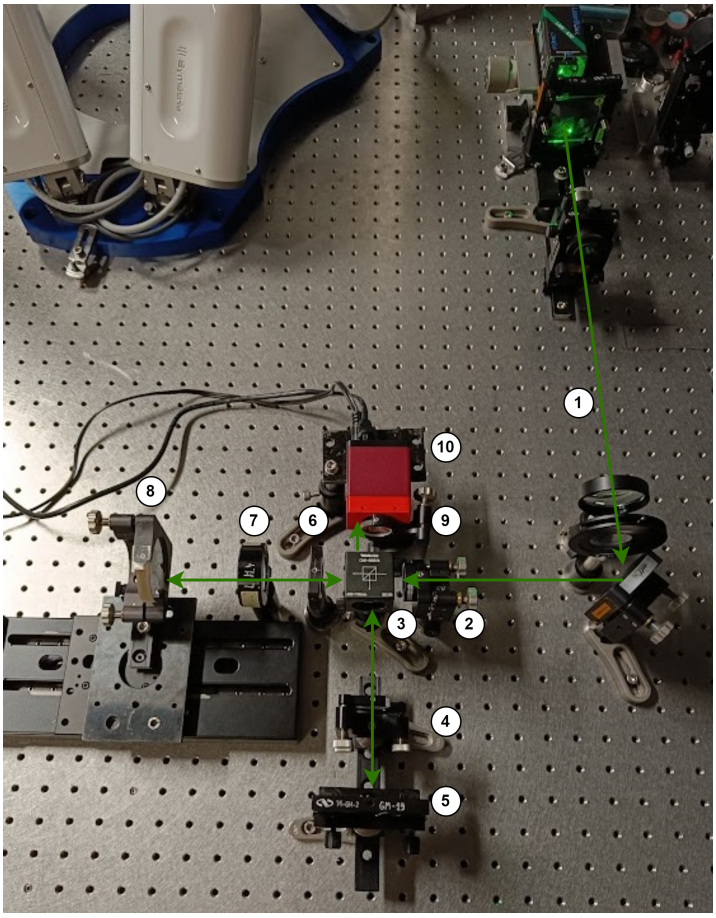

Figure 4. a) proof of concept of the metrology instrument to validate its measurement principle. (1) Spatial filtering and collimation of the source, (2) ground glass diffuser from Edmund Optics, (3) CBS 50/50, (4) lens L1, (5) measurement mirror, (6) optical phase mask, (7) lens L2, (8) reference mirror, (9) microlens array, (10) Allied Vision Prosilica GE-2040 1.2" Monochrome CCD Camera modified with 3D printed components.

large coherence, an Oxxius laser at 532 nm peak wavelength, to do the measurements. It should be noted that we did not include the optical phase mask on this first iteration of the optical layout due to the multiple unwanted interferences we had from light going through the mask a second time after reflecting on the reference mirror. Nevertheless, we already proved the working principle of the optical phase mask with a low-coherence source at reference.[10] Accordingly, with the proof of concept, we aimed to obtain a repetition of the interference pattern of the same spot observed on the mirror where each interference pattern is at the same OPD. We obtained the desired results after aligning the optical components and ensuring an equal interferometer arm's length. Those results follow the numerical simulation of Fig. 1 and are represented in Fig. 5.

Figure 6 includes the results obtained for different configurations of the optical layout to understand the importance of the position of the optical components and the influence of the diffuser.

4. DISCUSSION

The objective of our paper was to confirm the innovative measurement principle of the instrument. After introducing the theoretical concept, we did a numerical simulation of the optical layout, which results aligned with the theoretical concept. Next, we implemented the optical layout with a proof of concept at the laboratory. The results obtained with the proof of concept, illustrated in Fig. 5, validated the numerical simulations and, accordingly, the measurement principle of the instrument. Those results demonstrate how it is possible to obtain a

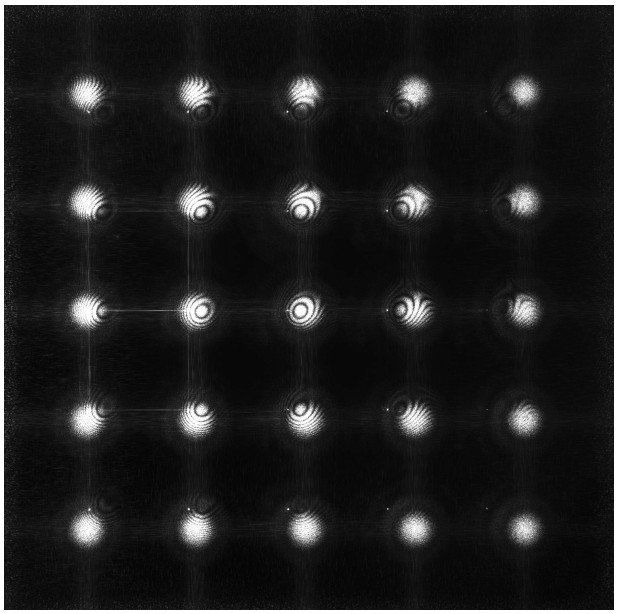

Figure 5. Illustration of the interference patterns measured at the detector on a single camera frame with the proof of concept. They represent a repetition of the interference pattern of the mirror's spot under characterization. Those results are according to the numerical simulations of Fig. 1 that aimed to prove the measurement principle of the instrument. With the interference patterns, we can reconstruct the local interferograms to determine the mirror's local topology and local induced vibration.

repetition of the interference pattern of the spot observed at the mirror on a single camera frame—one interference pattern associated with each microlense of the microlenses array. In Fig. 5, we can observe a decentering of the interference patterns, which we associate with a misalignment between the mirror's and microlenses' optical axes. As introduced in the previous section, we have to modify the optical path of the reference mirror to avoid the light going two times through the optical phase mask and to facilitate, accordingly, the alignment of the metrology instrument. We will study a second iteration of the metrology instrument in a future publication.

To illustrate the impact of the diffuser on the measurements, we studied four relevant configurations of the optical layout, which we presented in 6. In Fig. 6 a), we defocused the microlenses array to show how we can no longer distinguish the interference patterns but just the two superposed white spots from the two interference arms. When we removed the microlenses array, we detected a low contrast interference pattern according to Fig. 6 b). In contrast, when we defocused the microlenses array and removed the diffuser, we obtained an interference pattern like the one in Fig. 6 c). We got the same results without the lens L1 and L2. Each microlense images at the detector a portion of the interference pattern we would have detected if we did not have the microlenses array, like the full interference pattern of Fig. 6 d). The individual images are larger or smaller depending on the defocus of the microlenses array. We noticed how the interference pattern portion associated with each microlense is turned 180 degrees. When we reversed the individual images, we reconstructed a similar interference pattern to Fig. 6 d).

Regarding the measurement principle, we may need several camera frames to correctly distinguish a local induced vibration from a local change in the topology of the mirror. We will present the processing algorithms for interpreting the results in a future publication.

5. CONCLUSION

We demonstrated the innovative measurement principle of a metrology instrument to do real-time characterizations of the local topology and local induced vibrations of a mirror. For this demonstration, we used numerical simulations and developed a proof of concept of the instrument at the laboratory.

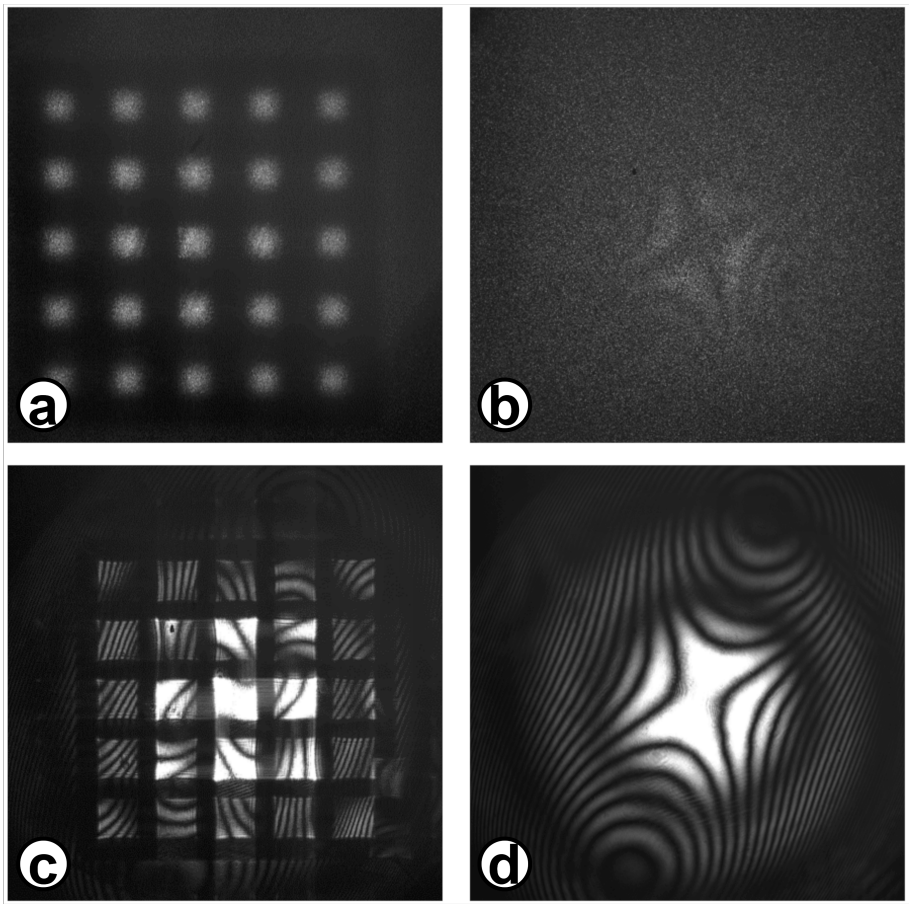

Figure 6. Image of the results measured at the detector for four relevant variants of the optical layout of Fig. 4 to illustrate the effect of the diffuser. (a) When we defocused the microlenses array, we no longer saw the interference patterns at the detector. (b) When we removed the microlenses array from the optical layout, we obtained a low-contrast interference pattern surrounded by speckle. (c) When we removed the diffuser from the optical layout and defocused the microlenses array, we noticed how each microlense imaged at the detector a portion of the interferogram we would have measured also removing the microlenses array, like the one of (d). (d) We measured a high-contrast interference pattern when we removed the diffuser and the microlenses array from the optical layout.

We tested the first iteration of the metrology instrument with a custom-made optical phase mask of 5 by 5 steps and a microlenses array of 5 by 5 microlenses. We presented the results obtained with a source of large coherence. We observed how we needed a more powerful white light source to improve the contrast and resolution of the results. Like for example, a Supercontinuum white light laser. We also discussed a second iteration of the metrology instrument to avoid the light going two times through the optical phase mask. It should be noted that a new optical phase mask is in development containing 49 steps in a 7 by 7 step square form or 49 interference patterns of the spot we observe on the mirror. This number of steps provides enough points for the data processing algorithms of the white light interferograms. For the moment, the size of the spot on the mirror that we can characterize is around 1 cm in diameter.

We developed the metrology instrument in the frame of the Einstein Telescope to characterize a suspended cryogenic mirror. However, the measurement principle is of extensive usability in other diverse applications related to real-time characterization of optical components with all the advantages of low-coherence interferometry.

ACKNOWLEDGMENTS

The E-TEST project is carried out within the framework of the Interreg V-A Euregio Meuse-Rhine Programme, with 7,5 million euros from the European Regional Development Fund (ERDF). By investing EU funds in Interreg projects, the European Union is investing directly in economic development, innovation, territorial development, social inclusion and education in the Euregio Meuse-Rhine .

REFERENCES

[1] Malacara, D., [*Optical Shop Testing*], Wiley-Interscience, 3 ed. (2006).

[2] Deng, Y. and Chu, D., "Coherence properties of different light sources and their effect on the image sharpness and speckle of holographic displays," *Scientific Reports* **7**, 1–12 (2017).

[3] Han, Z., Li, F., Chen, J., Rui, J., Wu, Z., Zhao, X., and Zhu, R., "All-fiber orthogonal-polarized white-noise-modulated laser for short-coherence dynamic interferometry," *Opt. Express* **31**(9), 14735–14749 (2023).

[4] De Groot, P., "Stroboscopic white-light interference microscopy," *Applied Optics* **45**, 5840–5844 (2006).

[5] Sandoz, P., Devillers, R., and Plata, A., "Unambiguous profilometry by fringe-order identification in white-light phase-shifting interferometry," *Journal of Modern Optics* **44**, 519–534 (1997).

[6] Groot, P. D., "Principles of interference microscopy for the measurement of surface topography," *Advances in Optics and Photonics* **7**, 1–65 (2015).

[7] Woo Jeon, J., Won Jeong, H., Bin Jeong, H., and Joo, K., "High-speed polarized low coherence scanning interferometry based on spatial phase shifting," *Applied Optics* **58**(20), 5360–5365 (2019).

[8] Sider, A., Fronzo, C. D., Amez-Droz, L., Amorosi, A., Badaracco, F., Baer, P., Bertolini, A., Bruno, G., Cebeci, P., Collette, C., Ebert, J., Erben, B., Esteves, R., Ferreira, E., Gatti, A., Giesberts, M., Hebbeker, T., van Heijningen, J. V., Hennig, J.-S., Hennig, M., Hild, S., Hoefer, M., Hoffmann, H.-D., Jacques, L., Jamshidi, R., Joppe, R., Kuhlbusch, T.-J., Lakkis, M. H., Lenaerts, C., Locquet, J.-P., Loicq, J., Van, B. L. L., Loosen, P., Nesladek, M., Reiter, M., Stahl, A., Steinlechner, J., Steinlechner, S., Tavernier, F., Teloi, M., Pérez, J. V., and Zeoli, M., "E-test: a compact low-frequency isolator for a large cryogenic mirror," *Classical and Quantum Gravity* **40**, 165002 (jul 2023).

[9] Sider, A., Amez-Droz, L., Amorosi, A., Badaracco, F., Baer, P., Bruno, G., Bertolini, A., Collette, C., Cebeci, P., Di Fronzo, C., Ebert, J., Erben, B., Esteves, R., Ferreira, E., Gatti, A., Giesberts, M., Hebbeker, T., Hennig, J. S., Hennig, M., Hild, S., Hoefer, M., Hoffmann, H. D., Jacques, L., Jamshidi, R., "lastName":"Joppe", "firstNames":"R.",, Kuhlbusch, T., Lenaert, C., Lakkis, M. H., Le Van, B. L., Loicq, J., Locquet, J. P., Loosen, P., Nesladek, M., Reiter, M., Stahl, A., Steinlechner, J., Steinlechner, S., Teloi, M., Vilaboa Perez, J., van Heijningen, J., and Zeoli, M., "E-test prototype design report," tech. rep. (2022).

[10] Vilaboa Pérez, J., Georges, M., Lenaerts, C., and Loicq, J., "Low coherence interferometry to characterize the induced vibrations and topology change of the cryogenic mirror of the Einstein Telescope prototype," *Advances in Optical and Mechanical Technologies for Telescopes and Instrumentation V* **121881E**(Proc. SPIE 12188) (2022).